THE JOURNAL OF PHYSICAL CHEMISTRY C

pubs.acs.org/JPCC Article

O_2 Activation over Ag-Decorated $CeO_2(111)$ and $TiO_2(110)$ Surfaces: A Theoretical Comparative Investigation

Luca Brugnoli, Alfonso Pedone,* Maria Cristina Menziani, Carlo Adamo, and Frédéric Labat*

Cite This: J. Phys. Chem. C 2020, 124, 25917−25930 Read Online

ACCESS | Metrics & More | Article Recommendations | Supporting Information

ABSTRACT: Periodic spin-polarized hybrid density functional theory calculations have been performed to investigate the reactivity of pristine, O-defective, and Ag-decorated $CeO_2(111)$ and $TiO_2(110)$ surfaces with a small Ag_{10} cluster toward O_2. The adsorption of O_2 and its subsequent dissociation have been studied in order to provide a better understanding of the role of the oxide, the metallic nanoparticle, and their interaction in the reactivity of composite metal/metal oxide materials toward O_2, as potential catalysts to this reaction. Structural, energetic, electronic, and vibrational properties of all species involved in the different reaction paths considered have been fully characterized. On the stoichiometric surfaces, Ag_{10} is oxidized and reduces surface Ce^{4+}/Ti^{4+} ions, while on the O-defective surfaces, the adhesion of silver is promoted only on CeO_2 but unfavored on TiO_2. On the other hand, on the silver-free supports, O_2 strongly adsorbs at vacancies and preferentially reduces to peroxide. When no O vacancies are considered on the Ag_{10}-decorated supports, the net positive charge on Ag_{10} actually prevents the adsorption and reduction of O_2. Instead, when O vacancies are included, two reaction pathways are observed; oxygen molecules can weakly absorb on the silver cluster as a superoxide moiety or strongly adsorb at the vacancy as peroxide. The dissociation of the O−O bond of the peroxide is favored both from the thermodynamic and kinetic points of view in silver-decorated surfaces, in contrast with the silver-free cases. In addition, Ag_{10}/CeO_2 shows higher activity toward the O_2 adsorption and dissociation than Ag_{10}/TiO_2, which can be related both to the higher ionicity and superior electron storage/release ability of ceria with respect to titania, thus leading to the weakening of the O−O bond and providing lower activation barriers for oxygen reduction. These results deepen the current understanding of the reactivity of metal/metal oxide composites toward O_2, especially elucidating how the surface stoichiometry affects the charge state of the metal clusters, and hence the reactivity of these interfaces toward O_2, with potential important consequences when such composites are considered for catalytic applications.

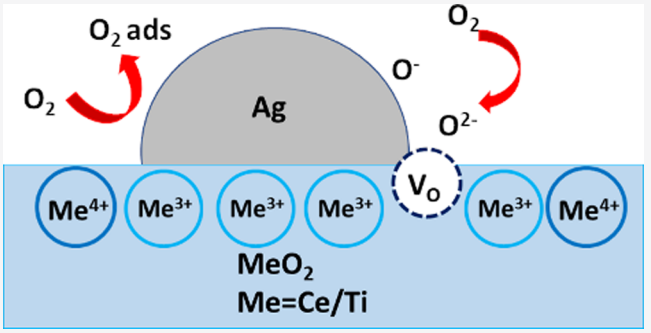

1. INTRODUCTION

Transition-metal nanoparticles (NPs) dispersed over metal-oxide supports constitute one of the main types of heterogeneous catalysts, with countless applications in many industrial and technological processes for the abatement of environmental pollutants produced by industrial activity and motor vehicles.[1−3] In particular, catalysts based on silver NPs supported at the oxide surfaces are appealing for their high activity in low-temperature oxidation processes[4−11] and their remarkable lower costs with respect to those based on gold and platinum, making them more suitable for large-scale applications.[7,12] It is known that the catalytic activity toward the oxidation of silver NPs supported on reducible oxides is enhanced[13] by the metal-support interaction effects which boost the reactivity of both the support and metal.[5,14,15] Among the reducible oxides, ceria (CeO_2) and titania (TiO_2) have been the most investigated ones in catalysis.[16] Although Ag/CeO_2 composites are known to be highly active for a huge number of catalytic reactions,[4,5,7,8,10,11,17,18] the Ag/TiO_2 composites have shown promising oxidant activity only recently.[4]

Two mechanisms have been proposed to explain the oxidation activity of these systems: one involves the release of O from the oxide lattice (Mars-van Kravelen, MvK) and the other involves the production of oxygenated species as peroxide (O_2^{2-}), superoxide ($^*O_2^-$), or atomic oxygen (O or $^*O^-$), when O_2 molecules interact with reactive sites (oxygen vacancy, oxide/metal junction, or metal particle surface) on the catalyst surfaces. These highly reactive oxygenated species react with the co-adsorbed substrate

Received: October 6, 2020
Revised: October 29, 2020
Published: November 15, 2020

https://dx.doi.org/10.1021/acs.jpcc.0c09080
J. Phys. Chem. C 2020, 124, 25917−25930

(Langmuir−Hinshelwood mechanism, LH) or the gas-phase substrate (Eley−Rideal mechanism, ER).[19,20]

The MvK mechanism involves the formation of an oxygen vacancy (V_O) at the oxide surface MO_2 (CeO_2/TiO_2), with the reduction of a couple of M^{4+}(Ce^{4+}/Ti^{4+}) cations to M^{3+}(Ce^{3+}/Ti^{3+}) for each neutral V_O formed.[21,22] Because this reaction modifies the stoichiometry of the catalyst, another mechanism is required to annihilate the vacancy; O_2 readily reacts at the vacancy site, oxidizing the surface and generating oxygen species able to react with the substrate following either the LH or the ER mechanisms. While the MvK mechanism is well characterized for CeO_2,[23] which is able to oxidize many species even without dopants or supported metallic phases, stoichiometric TiO_2 surfaces are quite unreactive toward the oxidation of CO,[16] but their reactivity can readily be boosted by the addition of dopants or metallic phases.[24,25]

The understanding of the reaction mechanism of these catalytic processes is of critical importance but is complicated by several critical parameters affecting the observed reactivity. In particular, one of the crucial steps is the activation of O_2 to form the reactive oxygen species which are then subsequently involved in the oxidative process. Several theoretical works, based on density functional theory (DFT) methods, have already investigated the interaction between O_2 and the main surfaces of these oxides, also considering additional supported silver clusters.[6,21,22,26−44,105] A direct comparison of the results obtained is however difficult due in particular to the different methodologies considered, as well as to the different structural models chosen in these works (supercell, slab size and slab thickness for instance). One of the main difficulties is the strongly correlated 3d and 4f states associated with the Ti^{3+} and Ce^{3+} ions, a characteristic of the reduced surfaces. Indeed, they are often described as largely delocalized by the most popular density functional approximations. A simple solution to this issue is the so-called DFT + U method, which uses a one-site potential, an additional term dependent on the Hubbard parameter U, to enforce the localization of the problematic 3d or 4f states.[45,46] Even though this method is computationally inexpensive, all the evaluated properties then depend on this parameter, including energies and structural parameters, making a comparison of results obtained with different U values difficult, even for systems based on the same oxide. On the other hand, although more computationally demanding, hybrid-DFT methods which include a certain amount of exact exchange, can be used to describe such systems in a more general way because they are applied on the whole system and not only to the problematic 3d or 4f states.[47,48] The same hybrid functional can then be applied to different materials with expected similar deviations for the computed properties, allowing a more consistent comparison of the results.[47] Furthermore, hybrid functionals are generally more accurate than DFT + U for both the insulating support and for the molecular species, even if their performances may decrease for conducting phases.[49,50]

In this work, we present a comprehensive investigation and comparison of Ag/CeO_2 and Ag/TiO_2 composites toward O_2, with the aim to highlight the differences and unravel the mechanisms of the catalytic activity of these two systems, using a periodic hybrid DFT approach. The most thermodynamically stable surfaces of the two oxides, CeO_2(111) and rutile TiO_2(110), were selected as supports for an Ag_{10} cluster. The silver/MO_2 junction is described in terms of adsorption energy, electronic structure, atomic charges, and spin polarization. Additionally, the effect of a surface vacancy, V_O, has been considered in the formation of the interface. Finally, the interaction with O_2 has been investigated for both silver-free and silver-decorated surfaces, highlighting the role of V_O and considering two pathways corresponding to the formation of the peroxo and superoxo species.

2. COMPUTATIONAL DETAILS

Spin-polarized DFT calculations have been performed with the *ab initio* CRYSTAL17 package,[51] adopting the global hybrid PBE0[52] functional with atom-cantered basis set constituted by Gaussian type functions. The choice of this functional is related to its good performances to reproduce many features of the bulk and surfaces of stoichiometric and defective cerium oxides [CeO_2, Ce_2O_3, and CeO_{2-x}(111)][53] and titanium oxides.[54−58]

A 2D supercell periodic approach has been used throughout this work. Models of the chosen $p(4 \times 4)$ slabs of CeO_2(111) and Ag_{10}/CeO_2(111) have been taken from a previous work.[55]

For TiO_2(110), a $p(5 \times 2)$ supercell, obtained from the PBE0 optimized bulk structure of rutile (a = 4.582 Å, b = 2.956 Å), has been considered. This supercell size has been chosen to be comparable with the supercell of CeO_2, in order to have similar distances between O vacancies and add-atom species in the periodic images of the cell, as already done in a similar comparative work.[56] Slabs with 2 O−Ce−O and 3 O−Ti_2O_2−O layers have been considered for CeO_2 and TiO_2, respectively. During geometry optimization, the bottom layer has been kept frozen at the bulk geometry, while the other layers and the add-atoms were free to relax. Default thresholds for convergence criteria have been considered.[57] To improve the description of the adsorption of the silver cluster and dioxygen, additional corrections for dispersive interactions have been taken into account with a semi-empirical D3 approach.[58,59]

The irreducible Brillouin zone was sampled with a regular Monkhorst-Pack grid 2 × 2 × 1 (4 **k** points) in both ceria and rutile systems. A threshold of 10^{-7} au has been used for the convergence of the total energy in the SCF procedure for all the single point energy and geometry optimization calculations, while a tighter value of 10^{-10} au was used for the transition state (TS) search and for the frequency calculations. The infinite lattice sums of the Coulomb and the exchange terms have been truncated with threshold values of 10^{-8}, 10^{-8}, 10^{-8}, 10^{-8}, and 10^{-20} for the CeO_2 containing systems, while the default threshold values 10^{-7}, 10^{-7}, 10^{-7}, 10^{-7}, and 10^{-14} have been found accurate enough for the TiO_2 containing systems.

As previously shown on cerium oxides,[53] well-converged structural properties can be obtained with a relatively small GTO basis set, tailored to describe the condensed phase, while energetics associated with the redox processes of interest may require a more extended and flexible basis set to reach convergence. Similar precautions have also been adopted for the couple Ti^{4+}/Ti^{3+} in hybrid DFT studies of doped TiO_2.[60] For the CeO_2-based systems, basis sets 1 (BS1) and 2 (BS2) from a previous work of some of us[55] have been used, here labeled $BS1_{CeO_2}$ and $BS2_{CeO_2}$. In both cases, the inner core of Ce has been described by a semi-relativistic effective core potential (srECP),[61] while the $4s^24p^65s^24d^{10}5p^66s^25d^14f^1$ electrons have been explicitly described with a (10sp8d8f)/[4sp3d3f] contraction scheme for $BS1_{CeO_2}$ and a larger

https://dx.doi.org/10.1021/acs.jpcc.0c09080
J. Phys. Chem. C 2020, 124, 25917−25930

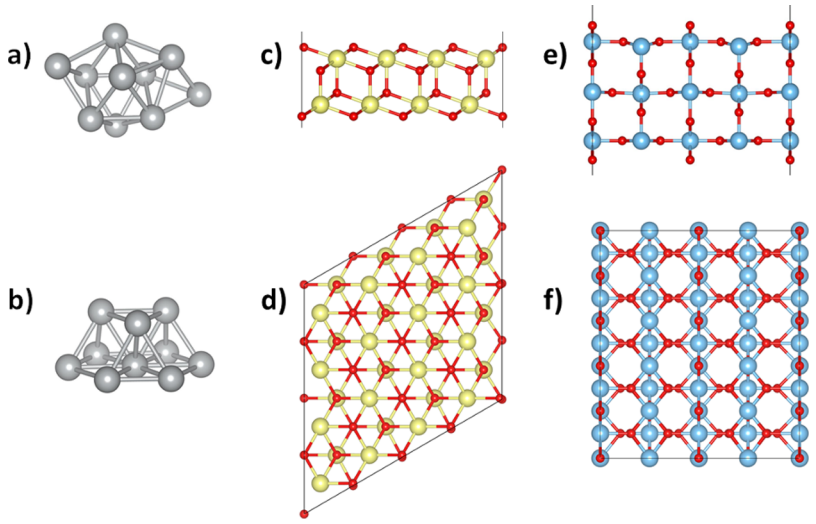

Figure 1. Gas-phase optimized (a) and hemispherical Ag_{10} cluster (b); side (c) and top (d) views of the $CeO_2(111)$ supercell; and side (e) and top (f) views of the $TiO_2(110)$ supercell. Grey, red, light yellow, and light blue balls represent the Ag, O, Ce, and Ti atoms, respectively.

(12s12p9d8f)/[8s7p4d4f] one for $BS2_{CeO_2}$. For O, a 8-411G(d) basis set with outer exponents re-optimized for bulk CeO_2 has been adopted for $BS1_{CeO_2}$[62] and the (13s7p2df)/[7s4p7p2df] contraction scheme has been selected for $BS2_{CeO_2}$.[63]

Similarly, for the TiO_2-based systems, two distinct basis sets have been employed; (i) $BS1_{TiO_2}$, in which Ti and O have been described with all-electron basis sets, with (20s12p4d)/[5s4p2d] and (14s6p1d)/[4s3p1d] contraction schemes, respectively, and exponents of the outer s, p, and d primitives optimized on the rutile and anatase structures[64] and (ii) $BS2_{TiO_2}$, where Ti is described by a larger basis set with a (20s12p6d3)/[5s4p4d] contraction scheme, obtained by removing the f primitive function from the original version[65] and including an additional diffuse d primitive with an exponent value of 0.12, along with the basis set previously described for $BS2_{CeO_2}$ for O.

On the other hand, for O_2, two distinct basis sets have been defined for the interaction with CeO_2 and TiO_2; the O basis used to describe the oxide anion has been modified by replacing the original exponent of the d primitive with 1.1. This choice provided the best agreement with the O−O bond length and binding energy computed with the O basis taken from BS2.

It is worth highlighting that the use of the customized basis set of the small size for the O in the two oxides allows the achievement of higher accuracy on the computed structural properties for both, while keeping the computational cost low. Then, the use of a common higher tier basis set for both CeO_2 and TiO_2 ensures a more consistent evaluation of the energetics of interest.

In all cases, Ag inner core electrons have been described by an ECP[66] and the valence electrons $4s^24p^65s^14d^{10}$ by a contraction scheme (6s5p5d)/[4s3p2d].[67]

$BS1_{CeO_2}$ and $BS1_{TiO_2}$ have been used to perform all geometry optimizations and subsequent frequency calculations at the Γ point to verify the minima and saddle-points localized. The $BS2_{CeO_2}$ and $BS2_{TiO_2}$ have been used to perform single point calculations on selected structures, pre-optimized with BS1, to compute reaction energies, Mulliken's charges, spin-populations, and DOSS. Basis set superposition error has been also considered by using the standard counterpoise approach,[68] when necessary. In addition, in the following, all energies reported include D3 corrections.[58,59]

To find TS, the distinguished reaction coordinate approach[69,70] has been used, by first performing a relaxed scan along a selected reaction coordinate and then by following uphill the lowest eigenvector of the Hessian matrix. All TSs reported in the following have a single imaginary frequency. To decrease the high computational cost related to the calculation of numerical frequencies, the Hessian matrix has been built considering only a fragment of the full system, corresponding to the first and second neighbors with respect to the adsorbed species, as already done in our previous work.[55]

The reduction of the oxide surfaces, either by V_O formation or by Ag_{10} adsorption, leads to the formation of radical species M^{3+} (and Ag_{10}^{3+}). Additionally, O_2 is treated in its ground state as a triplet. During the calculations, different magnetic solutions [ferromagnetic (FM) and antiferromagnetic] can be obtained, characterized by the number of unpaired electrons, the sites where they are localized, and their spin alignment. The energetic difference between these different solutions have been found to be negligible when compared to the reaction energies involved; therefore, only the FM solutions have been characterized throughout.

3. RESULTS AND DISCUSSION

In the following sections, the formation of the silver−metal oxide interface is first discussed. Then, the oxygen vacancy formation is described for both the silver-free and the silver-decorated surfaces. Lastly, the interaction of the different surfaces with O_2 is considered.

3.1. Ag_{10} on Stoichiometric Surfaces. The choice of a model cluster is a rather complex matter. With the present computational setting, the level of theory adopted, and the size of the supercells required to represent the oxide support, an Ag_{10}(7-3) model cluster has been chosen, as already used in previous studies[55,71] on CeO_2. The size is small enough to belong to the category of the nonscalable regime of properties, being the quantum effects associated with the variation of the

https://dx.doi.org/10.1021/acs.jpcc.0c09080
J. Phys. Chem. C 2020, 124, 25917−25930

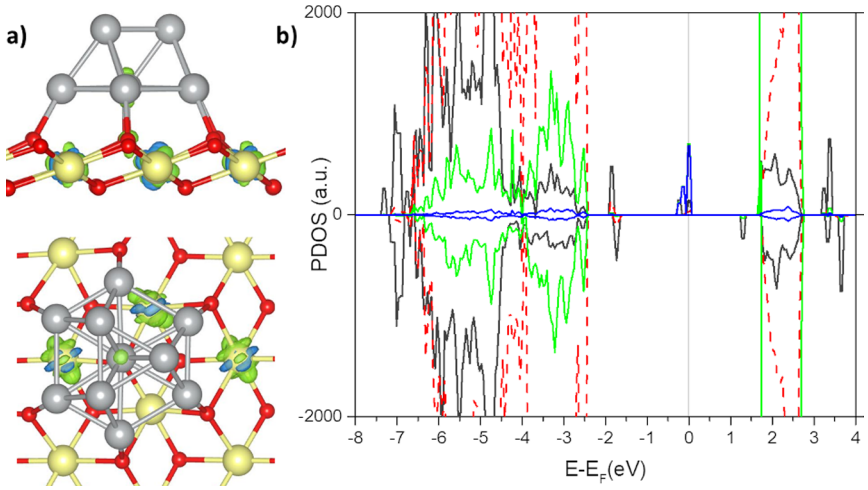

Figure 2. FM solution of $Ag_{10}/CeO_2(111)$: (a) top and side views of the spin-density map (isocontour value: 0.01 atomic unit). Green and blue correspond to positive and negative contributions, respectively; (b) total (black line) and atom-projection contributions to DOSs, with O, Ce (total), Ce^{3+}, and Ag contributions in red, green, blue, and grey, respectively. Positive and negative contributions correspond to α and β electrons, respectively.

number of atoms still relevant. Therefore, the results obtained should held more a qualitative value than quantitative.[72]

The cluster has been cut from bulk Ag along the 111 direction, and it is composed by two layers of 7 and 3 atoms (see Figure 1b). This hemispherical cluster, other than being a representative of the shape of larger silver NPs observed on both $CeO_2(111)$[10,73] and $TiO_2(110)$,[74,75] is rigid enough to keep the same atomic connectivity along the investigated reactions on both supports, allowing for a more consistent comparison of the key-step processes.

The adsorption of a metal cluster on an oxide surface can lead to a simple charge polarization because of the interaction between the metal and the surface oxygen, or to a net electron transfer (ET) from the metal valence to the low lying 3d/4f unoccupied states of the Ti^{4+}/Ce^{4+} ions,[76] which form the conduction band of the oxide. The adsorption energy has been computed as

$$E_{ads}(Ag_{10}) = E(Ag_{10}/MO_2) - E(MO_2) - E(Ag_{10}) \quad (1)$$

where $E(Ag_{10}/MO_2)$ is the energy of the relaxed silver/oxide system, $E(MO_2)$ is the energy of the relaxed oxide slab, and $E(Ag_{10})$ is the energy of the optimized cluster in gas phase (see Figure 1a). A negative value thus corresponds to a stable adsorption.

3.1.1. Ag_{10} on CeO_2. Experiments have shown that silver deposition on $CeO_2(111)$ induces the reduction of the oxide, but it was debated if this is due to a charge transfer from silver particles or from reverse spill-over of O from ceria to silver.[27,77,86,89] Previous theoretical results have confirmed the first hypothesis,[55,71,78−80] and the reverse O spill-over was found thermodynamically unfavored.[71]

In a previous work,[55] we have shown that Ag_{10} deposition on $CeO_2(111)$ occurs with the reduction of the oxide; about 0.4 eV favors the reduction of three Ce over the reduction of only two Ce, while several Ce^{3+} configurations were found to be almost degenerate. The most stable FM configuration obtained is reported in Figure 2, as well as the corresponding density of states (DOS). The unit cell contains 4 unpaired electrons, 3 localized on 3 Ce^{3+} in the cationic layer below the cluster and 1 on it, formally oxidized to Ag_{10}^{3+}, which is consistent with previous investigations.[71,78] Ce^{3+} and Ce^{4+} ions are distinguished by the net magnetization of the former close to unity (0.98−1.00 μ_B), as derived by the Mulliken's spin-population analysis. The DOS shows the occupied Ce 4f states at the top of the valence band, well above the top of the O 2p valence band from the O^{2-} ions and the bonding states Ag−O.

Ag_{10} has a good match with respect to the surface O layer of ceria, the cluster bottom layer stays flat with all the Ag in contact with one O ion, with an average Ag−O bond length of 2.18 Å, resulting in a binding energy of −5.60 eV.

3.1.2. Ag_{10} on TiO_2. Contrary to CeO_2, there is no conclusive experimental evidence about the reduction of the surface upon the deposition of silver particles for TiO_2. Some studies reported the reduction of the support, while others did not reveal changes in the oxidation states.[81−83] These controversial results are probably a consequence of the difficulty to obtain defect-free titania surfaces, which are less easily reduced by the metal deposition.

From a theoretical point of view, DFT models of atoms and small Ag clusters have been used to study the Ag/TiO_2 interface, mainly for rutile (110) and anatase (101). Not all these studies discussed whether the interface is formed with charge transfer or not. Some works did not consider the correction for the delocalization of 3d states,[83−87] preventing the localization of the transferred charge to Ti^{3+}. Others made use of the spin-restricted approach, which does not allow describing magnetic centers like Ti^{3+}[44] (and not only). Even when unrestricted calculations and localization potentials have been used, controversial results have been reported because ET from Ag to TiO_2 surfaces was not always observed.[88,89]

Here, the rutile (110) surface has been considered because it is the most thermodynamically stable and experimentally characterized one. The cluster was adsorbed maximizing the interaction between the basal atoms and the topmost twofold coordinated oxygen sites (O_{2c}) of the surface.

In contrast to the adsorption on CeO_2, a single self-consistent solution was found for Ag_{10} on TiO_2, characterized by the oxidation of the cluster to Ag_{10}^{3+} and the reduction of 3 Ti^{3+} in the second cationic layer of the support, in agreement with previous DFT + U calculations and some experiments,[89,90] as exemplified by the spin-density plot, as shown in Figure 3a. This is localized at the Ti^{3+} centers on the 3d

https://dx.doi.org/10.1021/acs.jpcc.0c09080
J. Phys. Chem. C 2020, 124, 25917−25930

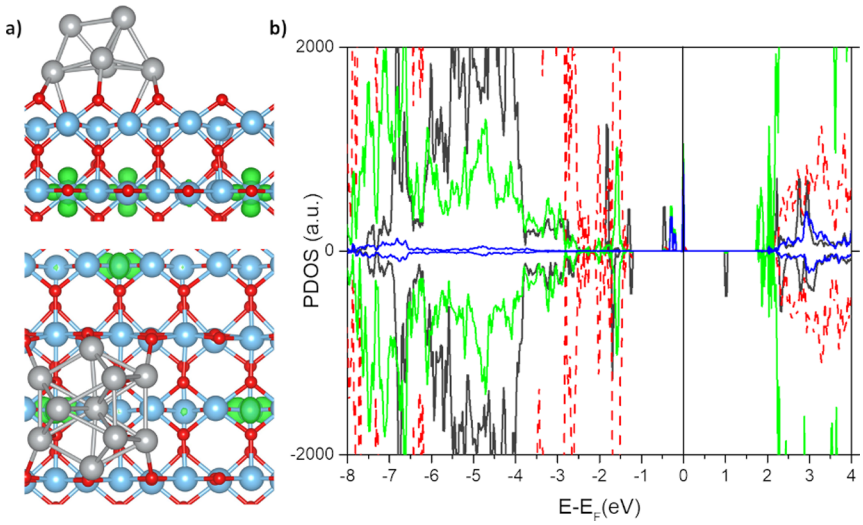

Figure 3. FM solution of $Ag_{10}/TiO_2(110)$: (a) top and side views of the spin-density map (isocontour value: 0.01 atomic unit) and (b) total (black line) and atom-projection contributions to DOSs, with O, Ti, Ti^{3+}, and Ag contributions in red, green, blue, and grey, respectively. Positive and negative contributions correspond to α and β electrons, respectively.

states, which appear in the main gap in the DOS of the oxide but close to the Ag−O bonding states[47] (Figure 3b). We note that several initial Ti^{3+} spatial configurations have been tested but the same final configuration has always been obtained.

From the data reported in Table 1, the cluster, formally +3, has a net charge of 1.68 |e⁻| and a magnetization of 0.88 μ_B. In the case of Ti^{3+} centers, the magnetization of the ions varies between 0.78 and 0.82 μ_B. The others formally Ti^{4+} possess a small magnetization between 0.01 and 0.03 μ_B for the ones in the first layer and between 0.07 and 0.10 μ_B in the second, while in the third, it is negligible. The difference with respect to the Ce^{3+} in CeO_2 is ascribed to the larger spatial extension of the occupied 3d orbitals of the Ti compared to the more localized 4f of Ce; therefore, the 3d orbitals on adjacent Ti sites participate in the formation of bands. The computed binding energy for the cluster is −5.04 eV, which is slightly less stable than in the CeO_2 case (−5.60 eV). This can be directly related to the reduced number of Ag−O bonds formed [6 for $Ag_{10}/TiO_2(110)$ and 7 for $Ag_{10}/CeO_2(111)$], which are also longer (2.23 vs 2.18 Å). Indeed, the adhesion energy per bond is 0.45 and 0.43 eV for CeO_2 and TiO_2, and the dispersion contributions are very similar in both cases.

Table 1. Computed Adsorption Energies (E_{ads}, in eV) of Ag_{10}, Average Bond Distance between the Basal Ag Atoms and the Surface O (R_{Ag-O}, in Å), Cluster Total Charge ($Q_{Ag_{10}}$, in |e⁻|) and Magnetization ($M_{Ag_{10}}$, in |μ_B|), for the Adsorption of Ag_{10} on the $CeO_2(111)$ and $TiO_2(110)$ Surfaces

system	nMe^{3+}	E_{ads}	R_{Ag-O}	$Q_{Ag_{10}}$	$M_{Ag_{10}}$
Ag_{10}/CeO_2	3	−5.60	2.177	1.379	0.849
Ag_{10}/TiO_2	3	−5.04	2.226	1.680	0.879

3.2. O Vacancy Formation. Oxygen vacancies (V_O) are the most common defects in reducible oxides as ceria and titania and they are well known to strongly affect the reactivity of these materials, even if for TiO_2 interstitial Ti can also play an important role.[76,91] These defects alter the oxide surface reactivity, promoting or hindering the adsorption of metal particles.[51] At the same time, the adsorbed metal affect the formation of the V_O, making the process more or less favored than on the metal-free surface.[92] The removal of an O atom from the lattice leaves two electrons behind, thus reducing the surface. According to most theoretical works, these electrons localize on the 3d/4f orbitals of the Ti/Ce around the V_O.[21,22]

Here, V_O has been modeled on the metal-free oxide surfaces, at the edge of the cluster oxide (interfacial O, O_I, see Figure 4), and on the surface site close to the cluster (surface O, O_S). The

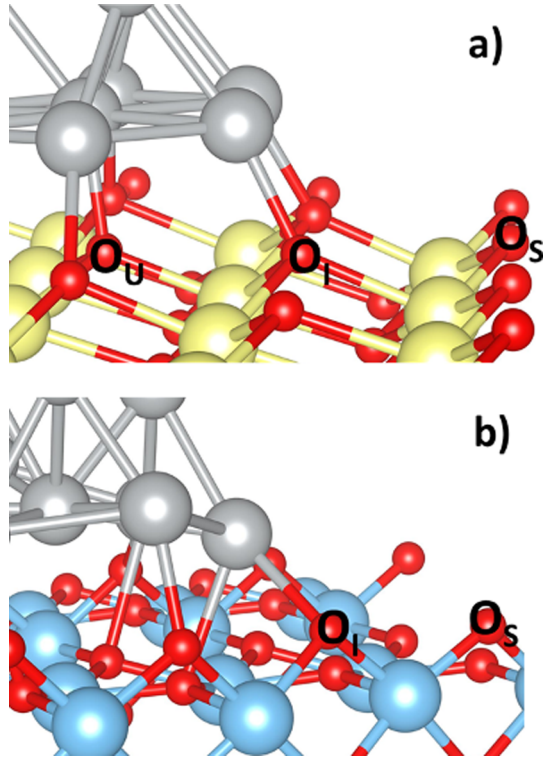

Figure 4. O sites selected for the surface (O_S), interface (O_I), and underneath (O_U) O vacancies on (a) $Ag_{10}/CeO_2(111)$ and (b) $Ag_{10}/TiO_2(110)$.

https://dx.doi.org/10.1021/acs.jpcc.0c09080
J. Phys. Chem. C 2020, 124, 25917−25930

formation energy of the vacancy, E_{fv}, has been evaluated adopting the following expression

$$E_{fv} = E(MO_{2-x}) + 1/2E(^3\Sigma_g^-O_2) - E(MO_2) \quad (2)$$

where $E(MO_2)$ is the energy of the stoichiometric surface, $E(MO_{2-x})$ is the energy of the surface with a V_O, and $E(^3\Sigma_g^-O_2)$ is the energy of the gas-phase O_2. The computed values for all systems investigated are reported in Table 2.

Table 2. Computed Formation Energies (E_{fv}, in eV) of the Surface V_O with Respect to $1/2O_2$ at Different Sites for the $CeO_2(111)$, $Ag_{10}/CeO_2(111)$, $TiO_2(110)$, and $Ag_{10}/TiO_2(110)$ Systems, along with the Number of M^{3+} Obtained (nM^{3+}, Me = Ce/Ti), the Average Spin Population of the M^{3+} Ions ($M_{M^{3+}}$, in $|\mu_B|$), and the Total Charge Associated to the Metal Cluster (Q_C, in $|e^-|$)

system	E_{fv}	nM^{3+}	site/configuration M^{3+}	$M_{M^{3+}}$	Q_C
CeO_2	2.72	2	$O_S/2_1-2_1$	1.003	
CeO_2	2.98	2	$O_S/1_1-1_1$	1.001	
Ag_{10}/CeO_2	3.18	5	$O_S/1_1-1_2$	1.000	1.35
Ag_{10}/CeO_2	3.51	4	$O_I/1_1$	1.001	0.93
TiO_2	2.84	2	$O_S/2_2-2_2$	0.834	
TiO_2	4.20	2	$O_S/2_2-1_1$	0.761	
Ag_{10}/TiO_2	3.89	4	$O_S/1_1$	0.820	1.20
Ag_{10}/TiO_2	3.40	4	$O_I/1_2$	0.872	1.22

3.2.1. CeO_2 and Ag_{10}/CeO_2. On $CeO_2(111)$, the surface V_O was found slightly less stable than the subsurface one.[93,94] The migration of the former to the subsurface position makes the vacancy not accessible to an adsorbate molecule such as O_2. Nevertheless, the surface sites are those involved in the oxidation following the MvK reaction mechanism. We have therefore limited our investigation to the surface V_O, which forms with the reduction of two Ce^{3+}. Many quasi-degenerate configurations exist for the couple of Ce^{3+}, of which the most stable is the 2_1-2_1 one,[95,96] which corresponds to both reduced ions in the first layer of the surface and in the second coordination shell of the vacancy site (see refs[19,71]). The formation energy of the V_O is 2.72 eV. The corresponding structure and DOSS are shown in Figure 5. The other configuration considered is the metastable 1_1-1_1 one, where both the ions are in the first coordination shell of the vacancy site, with an E_{fv} of 2.98 eV (see Figure S1, Supporting Information).

Similar to our previous investigation[55] on Ag_{10}/CeO_2, we sampled O_S and O_I sites and a site below the cluster, O_U. On the O_S site, V_O forms with the reduction of two Ce nearby, with a E_{fv} of 3.18 eV, which is 0.46 eV higher than on the Ag-free surface. For the O_I site, the extra charge localizes on a Ce next to the V_O (1_1 site) and on the cluster, which is formally reduced to Ag_{10}^{2+}, with an E_{fv} value of 3.51 eV. As for the last case, a V_O on the site underneath the cluster, O_U, is considered; as for at the O_I site, one Ce and Ag_{10} allocate the extra charge, while the E_{fv} decreases to 2.68 eV, about 0.35 eV below the reference one on the clean surface. The structures and associated DOSs for the three O vacancies considered on Ag_{10}/CeO_2 are reported in Figure S2.

These results therefore indicate that the silver cluster hinders the O_V formation along its perimeter, at least from a thermodynamic point of view. This is a short-range effect because the E_{fv} on the closest surface site not connected to the cluster, of 3.18 eV, is close to the reference values of 2.72 and 2.98 eV on the Ag-free $CeO_2(111)$. For the V_O at the O_S site, two Ce^{3+} are formed, as found on the clean surface, with higher E_{fv} because of the Coulombic repulsion between the neighboring Ce^{3+} couples. At O_I and O_U sites, a single Ce^{3+} is formed, while the other electron is withdrawn by the cluster, reduced to Ag^{2+}; the two defects have a similar reduction state, but the formation energies differ by about 0.8 eV. The difference can be rationalized with the higher stabilization of the cluster structure at the O_U site than at the O_I site.

The computed E_{fv} then indicate that silver deposition could be more stabilized on the O-defective surface when compared to the stoichiometric one depending on the site of adsorption. This is in agreement with experimental evidence that the adsorption energies increase with the degree of reduction of the surface.[97,98] From these data, it is therefore expected that oxygen defects act as anchoring sites for the silver particles, with potential high impact on O_2 reactivity.

3.2.2. TiO_2 and Ag_{10}/TiO_2. In the case of $TiO_2(110)$, the most reactive O is the undercoordinated bridging O_{2v}.[22] As for ceria, many electronic configurations of the reduced Ti^{3+} exist, with the most stable one found in the second cationic layer

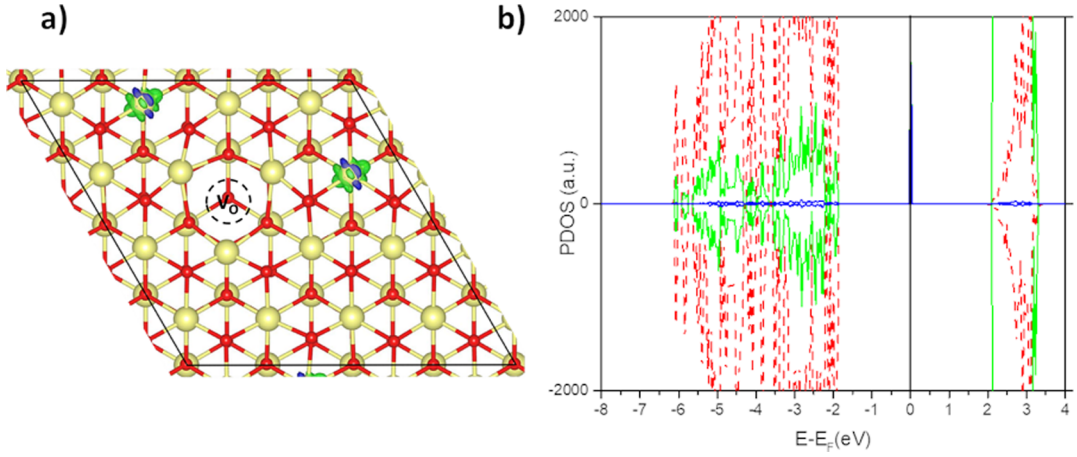

Figure 5. FM solution for the V_O at surface site of $CeO_2(111)$, with 2_1-2_1 configuration for the localized Ce^{3+} centers: (a) spin-density map (isocontour value: 0.01 au) and (b) atom-projection contributions to the DOSs. In green/blue, the positive/negative spin densities (isocontour value: 0.01 au). Positive and negative contributions correspond to α and β electrons, respectively.

https://dx.doi.org/10.1021/acs.jpcc.0c09080
J. Phys. Chem. C 2020, 124, 25917−25930

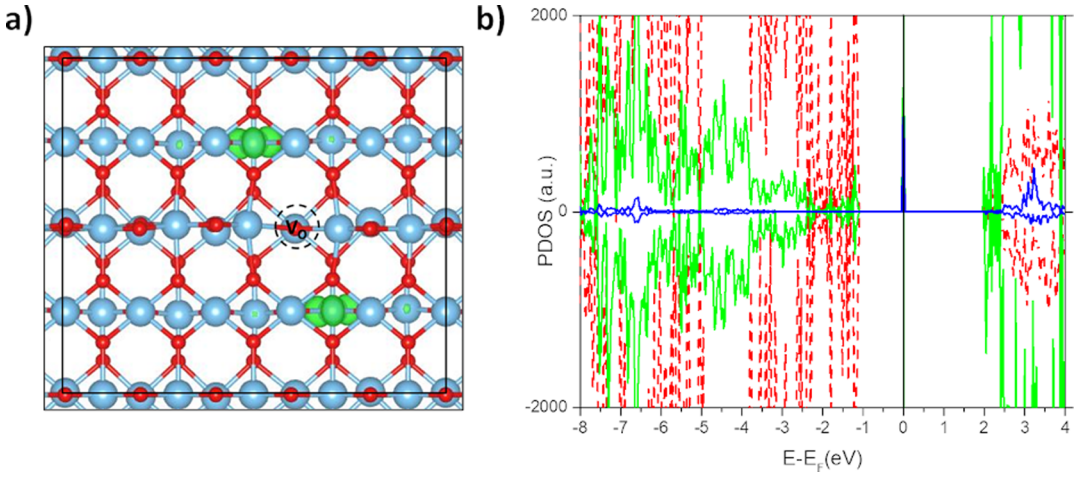

Figure 6. FM solution for the V_O at surface site O_{2c} $TiO_2(110)$, with a 2_2-2_2 configuration of the localized Ti^{3+} centers; (a) top view of the spin density map (isocontour value: 0.01 au) and (b) atom-projection contributions to the DOSs.

from the surface.[99−101] Because of the quasi-degenerate nature of these configurations, the ground state has not been identified unambiguously; the computed relative energies depend on several factors,[99] such as the supercell size, the number of $O-Ti_2O_2-O$ layers, the number of relaxed layers, the DFT model adopted, and the value of U_{eff}. As a consequence, several configurations are expected to be populated at finite temperatures, and the low barrier for the polaronic hopping of the 3d states on Ti^{3+} would make the interchange fast.[99] Because the spatial distribution of the Ti^{3+} is expected to affect the reactivity of the surface with O_2, it is necessary to consider the most stable positions.

We have characterized the ground-state configuration proposed in ref 101 with both Ti^{3+} sites in the second cation layer from the surface and from the vacancy, corresponding to a 2_2-2_2 configuration (see Figure 6). The computed E_{fv} is 2.84 eV, and the DOSS (see Figure 6, panel b) displays a sharp peak at the Fermi level, 1.20 eV above the top of the O 2p valence band.

An additional 2_2-1_1 configuration was also considered, where one Ti^{3+} has been transferred to the first cationic layer, in the first cationic shell of the vacancy (see Figure S3, Supporting Information). A E_{fv} value of 4.20 eV, which is 1.26 eV higher than the other case,[26] was obtained, confirming that the 2_2-2_2 configuration is the ground state one.

On $Ag_{10}/TiO_2(110)$, the V_O has been modeled at the O_S and O_I (see Figure 7). In both cases, the extra charge is localized on Ti in the first cationic layer and on the cluster, thus reducing to Ag_{10}^{2+}.

For the V_O at O_s, only Ti located at the 1_1 site is reduced, while the cluster reduced to Ag_{10}^{2+} incorporates the residual charge. Its charge and magnetization decreased, respectively, from 1.68 to 1.12 $|e^-|$ and from 0.88 to 0.04 μ_B. Similarly, the V_O at an interface site (O_I) forms with the reduction of a single Ti located at the 2_1 site and of the cluster (1.09 $|e^-|$). The vacancy formation energies are 3.40 and 3.89 eV for the O_S and O_I sites, respectively, thus, the vacancy formation is thermodynamically promoted along the rutile−silver interface when compared to the surface site nearby. In comparison to the clean $TiO_2(110)$ surface (E_{fv} = 2.84 eV), the V_O formation is hampered at both sites considered, indicating that the Ag particle binding is weaker on the reduced $TiO_2(110)$ surface. This destabilization arises from the repulsive interaction

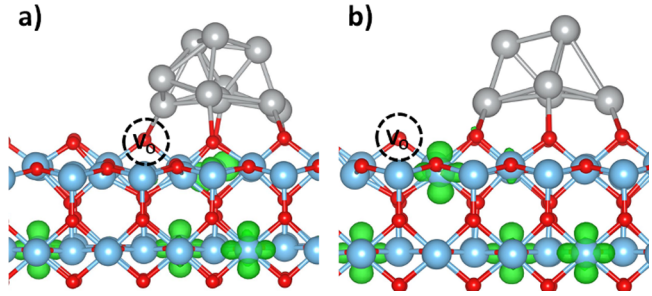

Figure 7. Spin density map (isocontour value: 0.01 atomic unit) of the FM solutions for the O vacancy at interface site O_I (a) and at surface site O_S (b).

between the Ti^{3+} ions; at the increase of their concentration, the surface Ti site reduction became favored with respect to the subsurface ones.[22]

3.3. O_2 Reactivity on Ag-Free Surface. *3.3.1. $CeO_2(111)$ and $TiO_2(110)$ Surfaces.* The first step in the O_2 activation involves the interaction between the gas phase and the oxide surface, which must be electron rich in order to reduce O_2; on the stoichiometric surfaces, the physisorption of O_2 occurs only at cryogenic temperature.[102,103] Without dispersion corrections, the computed adsorption energies are negligible, −0.02 eV for both ceria and titania in close agreement with previous calculations (PBE and PBE + U).[26,35] By including the dispersion corrections, the stability of the adsorbates increases to −0.16 and −0.21 eV for ceria and titania, respectively. The corresponding structures and DOSS are reported in the Supporting Information in Figures S4 and S5.

3.4. O_2 Reactivity on O-Defective Surfaces. As anticipated, defective surfaces are much more reactive toward O_2 than stoichiometric surfaces: the O_2 fills the vacancy site, independently from the position of the reduced centers. During adsorption, an ET occurs from the defect states 4f/3d of Ce^{3+}/Ti^{3+} to the partially empty π^*_{2p} orbitals of the O_2 molecule, with the formation of either a superoxide (O_2^-) or a peroxide (O_2^{2-}), depending if the V_O acts as a one or two electron donor.

The product of the interaction O_2-V_O depends on the distance of the reduced cations and on the magnetization/spin multiplicity of the unit cell. With 4 unpaired electrons in the unit cell, the product can be in a quintet, a triplet, or a singlet

https://dx.doi.org/10.1021/acs.jpcc.0c09080
J. Phys. Chem. C 2020, 124, 25917−25930

state. For the quintet, the pairing of the radical centers is forbidden, and neither ET nor physisorption occur (at the V_O site). For the triplet, only the product of the mono ET, the superoxide O_2^-, is allowed. For the singlet, two distinct solutions can be found, an open-shell diradical as for the triplet but with opposite spin orientations or the closed shell product of the double ET, yielding peroxide O_2^{2-}. Both the O_2^{2-} products of the double ET and the open-shell $O_2^- - Ce^{3+}/Ti^{3+}$ can form, but the latter can be isolated only if the distance between the radical centers is large enough. Because of the reduction, the O−O bond is elongated and weakened; while one O refills the V_O, the other can be transferred to a substrate or migrate on the surface. The 4f and 3d defect states associated with Ce^{3+} and Ti^{3+} lie at lower energy than the unoccupied π^*_{2p} orbitals of O_2, the ET then occurs (quantitatively) with the equilibration of the energy levels of the donor and acceptor, through orbital interactions.

3.4.1. CeO_2(111). On polycrystalline samples of ceria, both reduced dioxygen species have been characterized by vibrational and EPR spectroscopies.[87,90,91] Instead, well-defined single crystals and nanoshaped particles exhibit different reactivity toward O_2, as was recently reported.[33,55,104] On the other hand, on single crystal CeO_2(111), neither peroxo and superoxo species are observed at a temperature as low as 81 K, due to the preference of the Vo for the subsurface sites, not accessible to O_2.[33] In addition, on NP-terminated (111) surfaces, containing both surface and subsurface V_O, only peroxide is observed, likely due to the short lifetime of the superoxide.[34] Indeed, DFT + *U* calculations found the reduction of O_2 to O_2^- adsorbed on the Ce^{3+} near the vacancy, and a barrier of only 0.35 eV for the migration and reduction into the vacancy to O_2^{2-}, driven by the high exothermicity of the process.[106] According to Conesa,[27] the superoxide can be isolated only for single electron donor defects on CeO_2(111), as for V_O paired with trivalent dopants.

Most of the earlier DFT investigations[26−28] have found the ET occurring only if the O_2 adsorbs directly into the V_O; any other adsorption sites (on top of Ce^{4+} or Ce^{3+} in 2_1 or 1_1 to V_O) resulted in weak physisorption, with only a small charge polarization of the molecule. Other works have shown the reduction of the side-on O_2 adsorbed on the Ce^{3+} (in 2_1) to superoxide.[33,106] Here, the study of the adsorption is limited to the end-on approach of O_2 to the V_O because it has already been shown to be the most favored one.[28] Computed data are collected in Table 3.

The 2_1-2_1 configuration used act as a one electron donor, providing the superoxo product (see Figure S6, Supporting Information). Instead, here, in the metastable 1_1-1_1 configuration, O_2 is found fully reduced to peroxide with the pairing of all radical centers and an adsorption energy 1.32 eV larger than the superoxo product. This is in agreement with the experimental observations and might indicate that the superoxide is only a short-life intermediate.[34] The barrier associated with the second ET should be close to that of the polaron hopping for the Ce^{3+} as measured in the bulk (about 0.5 eV[107]), which is overcome at room temperature.

The dissociation of the O−O is considered only for the peroxide case, which is equivalent to the migration of an adsorbed O on the stoichiometric surface.[77,96,104,105]

From the reaction path reported in Figure 8, the O bound to the surface moves toward one of the 2 equiv neighboring Ce

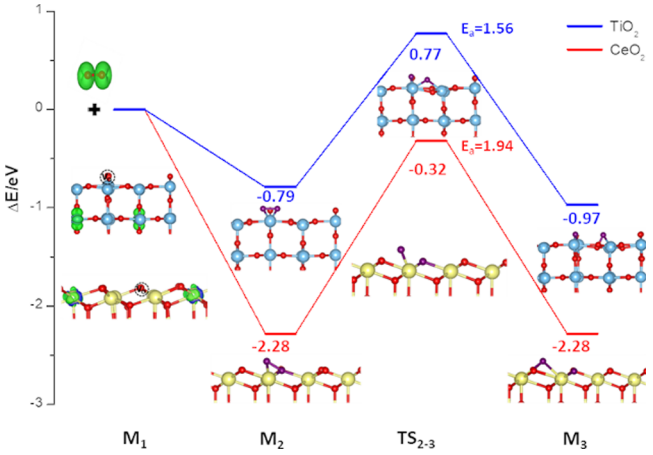

Figure 8. Comparison of the reaction path for the O_2 adsorption as a peroxide and following dissociation at a vacancy site on CeO_2(111) (red line) and TiO_2(110) (blue line). In green/blue, the positive/negative contributions to the spin-density (isocontour value: 0.01 au).

and, after crossing a TS (ν_i = −552 cm^{-1}), it is transferred to another surface O to form another peroxo moiety, equivalent to the starting one. Thermal activation is required to overcome the large activation barrier E_a of 1.96 eV, which is about 0.5 eV higher than the one already reported at the PBE and PBE + *U* levels.[26]

3.4.2. TiO_2(110). On O-defective rutile (110), O_2 interacts strongly with the surface vacancy and may form adsorbed superoxide, peroxide, or dissociated oxide ions (O^{2-}).[22] While the latter process seems thermodynamically more favorable, according to DFT calculations and in agreement with the STM observations,[108] there is no clear experimental evidence about the preferred reduction state of the adsorbed O_2 on rutile (110).

Previous pure DFT calculations (PW91) have shown that the peroxide product is more stable than the superoxide one[37] but lower barriers have been computed for migration and dissociation for this latter, closer to the experimental observations.[102,109−111] However, the stabilization of the superoxide can also be ascribed to multiple O_2 molecules adsorbed at the vacancy site, observed also at cryogenic temperature,[16] able to share the excess of charge ($2e^-$) of the vacancy site on the surface, therefore being detectable as a superoxide.[102]

As done for CeO_2, here, a single O_2 molecule is considered as interacting with the active V_O site; O_2 adsorbs at the bridge O_{2c} V_O (2_2-2_2 configuration) with a side-on orientation with respect to the surface, corresponding to the most stable configuration previously reported.[35,112]

Table 3. Computed Formation Energies of the V_O (E_{fv}, in eV), Adsorption Energies of O_2 as a Peroxide ($E^{O_2}_{ads}$, in eV), Sum of Mulliken Atomic Charges on O_2 (Q, in $|e^-|$), and Interatomic O_2 Distance (d_{O-O}, in Å)

System	E_{fv}	$E^{O_2}_{ads}$	Q	d_{O-O}
CeO_2	2.98	−2.28	−1.19	1.465
Ag_{10}/CeO_2 O_I	3.51	−3.12	−1.32	1.496
TiO_2	2.84	−0.79	−0.94	1.418
Ag_{10}/TiO_2 O_I	3.40	−1.64	−1.03	1.443

https://dx.doi.org/10.1021/acs.jpcc.0c09080
J. Phys. Chem. C 2020, 124, 25917−25930

The reduction to peroxide is obtained with the oxidation of both the Ti^{3+} and the final structure results in a closed shell singlet; a double ET occurs even if the electron donors are not directly adjacent to the V_O but quite far (5.7 Å) from the vacancy site, which is in agreement with the low activation energies found for the charge diffusion on rutile.[22] In contrast to ceria, where the ET can occur only from the 4f orbitals of Ce^{3+} ions to the $2\pi^*$ orbitals of the O_2 molecule, in titania, the transfer could also occur from the 3d orbitals of Ti^{3+} to the conduction band and finally to the O_2 molecule because the $2\pi^*$ orbital overlap with the conduction band (see Figures S5 and S7, Supporting Information). The single ET which provides the adsorbed superoxide is obtained for the triplet solution, by constraining **M** to 2 μ_B to prevent the pairing of the radicals localized on Ti^{3+} and on O_2^-. The computed adsorption energies confirm the peroxide as being more stable, with −0.79 and −0.09 eV values for O_2^{2-} and O_2^-, respectively.

The O−O dissociation of the peroxide product is then considered; one O adsorbs at the O_{2v} site while the other moves toward the Ti_{5v} site, crossing a TS (ν_i = −673 cm^{-1}) with an activation barrier E_a of 1.56 eV. This barrier is about 0.3 eV higher than the one reported previously at the PW91 level.[37] The dissociation process is slightly exothermic, with a reaction energy of −0.20 eV.

3.5. O_2 on Ag_{10}/CeO_2 and Ag_{10}/TiO_2. After discussing the possible interaction modes of O_2 with the Ag-free surfaces, the Ag_{10}-decorated supports are now considered, first with the stoichiometric case and then considering defective surfaces.

3.5.1. Stoichiometric Ag_{10}/CeO_2 and Ag_{10}/TiO_2. For both systems, adsorption of O_2 does not take place over the supported cluster (see Figure 9), O_2 slides toward the support, where it is weakly bound, with adsorption energies of −0.16 and −0.19 eV in the CeO_2 and TiO_2 cases, respectively. The same geometry is obtained when starting from different adsorption sites, including the top and the side of the cluster, as well as on the top of the surface Me^{3+} center.

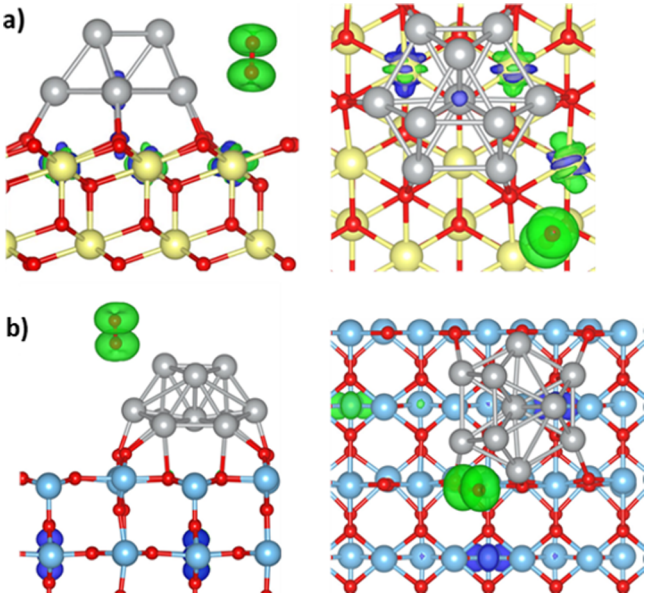

Figure 9. Side and top views of O_2 adsorbed on stoichiometric (a) Ag_{10}/CeO_2 and (b) Ag_{10}/TiO_2. In green/blue, the positive/negative contributions to the spin-density (isocontour value: 0.01 au).

The positive charge of Ag_{10} does not favor the adsorption of the electrophilic O_2, which instead is drawn toward the oxide surface. No charge transfer from the support to oxygen is found, at least for the sites considered. The electron donor Ce^{3+} and Ti^{3+} are either too close to the cluster or too deep inside the surface to interact efficiently with the O_2 molecule. In previous studies, O_2 adsorption at isolated Ce^{3+} has been shown to form O_2^-,[26,33] with a modest increase of the binding energies when compared to the fully oxidized surfaces. However, there is no experimental evidence for the formation of the superoxide on reduced $CeO_2(111)$,[33] at least at a detectable level, which might indicate that previous computational results underestimated the barrier of the ET from Ce^{3+} to O_2.

Our results on the $Ag_{10}/CeO_2(111)$ system are in apparent contrast with those found on the $Ag_1/CeO_2(111)$ system in a previous work,[32] where the O_2 adsorption (without reduction) on the supported Ag^+ was found to be favored when compared to the ceria support. This difference may arise from the fact that Ag^+ is a closed-shell species and Ag_{10}^{3+} a radical one (doublet); the bounding of the diradical O_2 with Ag^+ is allowed, while it is repulsive with Ag_{10}^{3+}. Size-effects may also play a role, with the particle being so small that also reactivity may greatly change with the numbers of atoms in the cluster.

3.5.2. O-Defective Ag_{10}/CeO_2 and Ag_{10}/TiO_2. Here, we will discuss the interaction of O_2 on Ag/MO_2 systems in the presence of an O_I vacancy. Although the computed E_{fv} values indicate that the O removal is not necessarily thermodynamically favored by the presence of silver, experimental evidence on Au-based oxidizing catalysts indicate that peripheral sites to the metal cluster react more readily with the substrate, according to a metal-assisted MvK mechanism.[113] The adsorption of O_2 has been considered at both the cluster side and on the V_O. On the cluster, the favored adsorption sites are the more electron-rich Ag atoms, as found by previous investigations.[44] On both supports, the undercoordinated Ag next to the V_O hold a slightly negative charge; here, the side-on adsorption of O_2 occurs, then partially reduces to superoxide. The corresponding structures are shown in Figure 10.

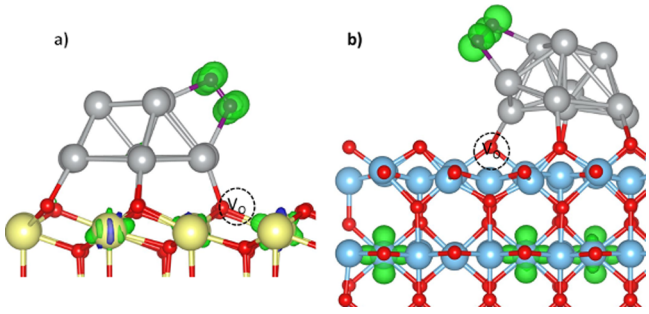

Figure 10. O_2 adsorbed as a superoxide on the cluster, next to the O_I vacancy on (a) Ag_{10}/CeO_2 and (b) Ag_{10}/TiO_2. In green/blue, the positive/negative contributions to the spin density (isocontour value: 0.01 au).

The stability of the adsorbate is similar for the two supports, with computed E_{ads} values of −0.51 and −0.42 eV on CeO_2 and TiO_2, respectively. The main difference between the two systems concerns the electron donor ability; on CeO_2, Ag_{10}^{2+} is oxidized to Ag_{10}^{3+} and on TiO_2, instead, the charge flows from the Ti^{3+} atom closest to the surface to the adsorbed O_2, through the cluster, which formally is still Ag_{10}^{2+}. This

https://dx.doi.org/10.1021/acs.jpcc.0c09080
J. Phys. Chem. C 2020, 124, 25917−25930

highlights a higher tendency of $TiO_2(110)$ to release the excess of charge received from Ag_{10} and the V_O. On the other hand, $CeO_2(111)$ shows a lower propensity to be re-oxidized. The Ag_{10}^{2+}/CeO_2 system seems to be able to reduce O_2 without involving Ce^{3+} ions following the reaction $Ag_{10}^{2+} + O_2 \rightarrow Ag_{10}^{3+} + O_2^-$.

In both cases, V_O then makes the cluster more electron rich, enabling the partial reduction of O_2 to O_2^-.

The second case considered is the O_2 absorption at V_O to fill the cavity, as described for the Ag-free surfaces. O_2 inserts into the vacancy with an end-on orientation, with the bottom O occupying the vacancy and the topmost O interacting with the cluster. In both cases, V_O acts as a double electron donor, yielding the O_2^{2-} and the oxidation of one Ce^{3+}/Ti^{3+} and of Ag_{10}^{2+} (see Figure 11, panels associated to M_2). The

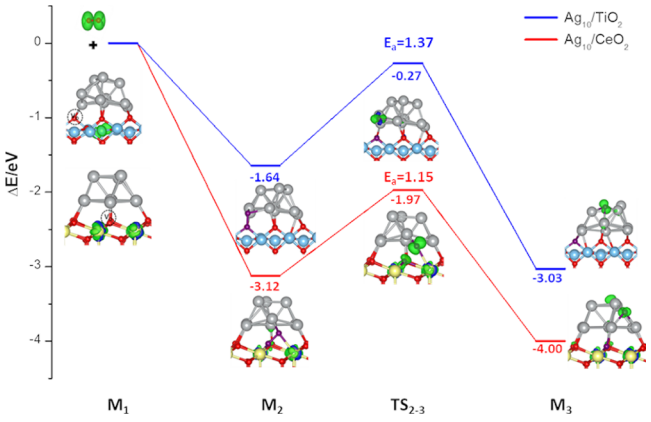

Figure 11. Energy profiles for the reaction paths of O_2 adsorption and dissociation at O vacancy sites on Ag_{10}/CeO_2 and Ag_{10}/TiO_2. In green/blue, the positive/negative contributions to the spin density (isocontour value: 0.01 au).

comparison of the processes at the vacancies on the bare support and at the O_I sites revealed a higher affinity of O_2 for the latter sites, with higher adsorption energies and charge transferred to the molecule, as reported in Table 2. In addition, the O−O bond lengths are more stretched at the interface V_O, and thus more prone to dissociate.

To further investigate this point, the dissociation of the peroxide at the interface has been considered. A relaxed scan of the O−O bond length has been performed to approximate the minimum energy reaction path and to locate a preferential site of adsorption of O on the cluster. Figure 11 shows the reaction energy profile considered along with the structures of the minima and TS obtained.

The TS corresponding to the dissociation, TS_{2-3}^{Ag/CeO_2} and TS_{2-3}^{Ag/TiO_2}, are characterized by imaginary frequencies of −421 and −352 cm^{-1}, respectively. The corresponding E_{a2-3} activation energies of 1.21 and 1.37 eV for CeO_2 and TiO_2, respectively, confirm the lowering of the O−O dissociation barriers when compared to the bare surfaces case. For both dissociation products (M_3), the upper O binds on a threefold site of Ag_{10}, while the bottom O binds to the cluster basal Ag as on the stoichiometric structures. The cluster is oxidized to Ag_{10}^{3+} and the upper O is reduced to the radical anion O^-, another reactive but elusive oxidant species.[114,115] The dissociation energies ΔE_{2-3} of −0.83 and −1.66 eV on CeO_2 and TiO_2, respectively, are much more exothermic than on the corresponding bare surfaces, in line with the higher affinity of O for Ag than for the stoichiometric surfaces. This is further confirmed by comparing the atomic O binding energies at different sites of the stoichiometric systems MO_2 and Ag_{10}/MO_2. This binding energy has been computed using the following formula

$$E_O^{ads} = E_{surface} + E_O^{gas} - E_{surface\text{-}O} \quad (3)$$

where $E_{surface-O}$ is the energy of the structures indicated as M_2 and M_3 (see Figures 5 and 8), $E_{surface}$ is the energy of the defect-free surfaces, and E_O is the energy of the isolated O atom ($^3P_2$ ground state).

Moving from the clean surface to the cluster/oxide O_I interface and finally to the cluster, the binding energies varies from −2.19 eV ($E_O^{CeO_2-M_2}$) to −2.28 eV (E_O^{Ag/CeO_2-M_2}) and finally to −3.16 eV (E_O^{Ag/CeO_2-M_3}) in the case of ceria. On titania, instead, the E_{ads} varies from −1.47 eV ($E_O^{TiO_2-M_2}$) to −1.73 eV (E_O^{Ag/TiO_2-M_2}) to −3.22 eV (E_O^{Ag/TiO_2-M_3}). The comparison shows that the affinity for O is clearly greater for the CeO_2 surface. For both cases, the adsorption at the Ag/MO_2 interface is only slightly enhanced with respect to the bare surface, and the adsorption on the cluster provides similar results. The driving force for the O−O dissociation is thus the stabilization of O on Ag. While this step is more thermodynamically favorable on the TiO_2 support, the O−O bond is more stretched at the interface Ag_{10}/CeO_2 because of the higher reduction degree of the molecule.

This might be related to the intrinsic properties of the surface morphology and electronic structure. First, the V_O in ceria is a stronger reducing site, the O_2 reductive adsorption is favored on the ceria support, where the $E_{ads}^{O_2}$ almost compensates the E_{fv}, in clear contrast with the TiO_2 case. The magnetic moment of O_2 is completely quenched, therefore behaving like a peroxide, but the charge acquired on the ceria support is larger than on titania, making the O−O bond weaker, as suggested by the larger interatomic distance (see Table 2). In presence of silver, V_O is more electron rich, and additional charge is then transferred to O_2, with similar contributions from the support in both cases, further weakening the O−O bond. The dissociation barrier is smaller on Ag_{10}/CeO_2, with much larger decrease from the clean surface because a different and shorter pathway occurs.

4. CONCLUSIONS

Periodic spin-polarized hybrid DFT calculations have been carried out to characterize the adsorption of an Ag_{10} cluster on $TiO_2(110)$ and $CeO_2(111)$ surfaces, the formation of surface oxygen vacancies along with the adsorption and dissociation of O_2 on the different surfaces considered.

The supported Ag_{10} injects electrons to both supports, with the reduction of three Ce^{4+}/Ti^{4+} to Ce^{3+}/Ti^{3+}. The resulting adhesion favored on $CeO_2(111)$, due to a more efficient Ag−O interaction between the basal Ag_7 plane and the O terminated surface. The silver deposition decreases the reducibility of the supports, making the formation of the V_O on the surface and interface sites more endothermic than on the silver-free surfaces, with a more pronounced effect on TiO_2.

Only a weak adsorption of O_2 on vacancy-free surfaces could be obtained because the reduced centers are not accessible to O_2, being located below the cluster (CeO_2) or in subsurface positions (TiO_2). The adsorption does not even occur on the

https://dx.doi.org/10.1021/acs.jpcc.0c09080
J. Phys. Chem. C 2020, 124, 25917−25930

silver cluster, formally oxidized to Ag_{10}^{3+}, which does not bind the molecule.

It should be noted that these results hold for ideal conditions as at 0 K and extremely low P of O_2; at higher T, the excess of charge is dynamic, as well as the cluster structure, allowing for more favorable interactions with O_2 for the ET. If photoexcitation is considered, then the extra charge trapped in the Ti 3d and Ce 4f states can be excited to the conduction band and transferred to O_2 without the requirement of a tight contact with the reactive centers.

We observed that oxygen vacancies are extremely reactive toward O_2, promoting the reductive adsorption. The complete reduction to peroxide O_2^{2-} is thermodynamically favored with respect to the partial reduction to O_2^-. This process is favored at V_O on the ceria support because of a larger charge transfer from the defect to O_2 in comparison with the V_O on the titania. The O−O bond dissociation of the peroxide product has then been considered and we found that on the bare surfaces the process is isoenergetic (CeO_2) or slightly exothermic (TiO_2) and highly kinetically hindered, with barriers between 1.50 eV (TiO_2) and 2.00 eV (CeO_2). At the edge sites of the cluster, instead, the dissociation is largely exothermic, with barriers of 1.15 and 1.37 eV for CeO_2 and TiO_2, respectively. The driving force of the process of dissociation of the peroxide is the healing of the vacancy and the transfer of the additional O to the cluster, forming the elusive radical ion O^-.

In conclusion, the presence of an O vacancy is mandatory to get the full reduction of the O_2 molecule, although no clear evidence could be obtained indicating that the deposited silver cluster could kinetically promote these defects.

■ ASSOCIATED CONTENT

Supporting Information

The Supporting Information is available free of charge at https://pubs.acs.org/doi/10.1021/acs.jpcc.0c09080.

Spin density maps for the metastable 1_1-1_1 Ce^{3+} configuration of the V_O on $CeO_2(111)$ and the metastable 2_1-1_1 Ti^{3+} on $TiO_2(110)$; spin density maps and DOSs for different V_O sites on Ag_{10}/CeO_2; spin density maps and DOSs for O_2 adsorbed on stoichiometric $CeO_2(111)$ and $TiO_2(110)$; and spin density maps and DOSs for partially reduced O_2 on O-defective $CeO_2(111)$ and $TiO_2(110)$ (PDF)

■ AUTHOR INFORMATION

Corresponding Authors

Alfonso Pedone − *Dipartimento di Scienze Chimiche e Geologiche, Università di Modena e Reggio Emilia, I-41125 Modena, Italy;* orcid.org/0000-0003-3772-7222; Email: alfonso.pedone@unimore.it

Frédéric Labat − *Institute of Chemistry for Health and Life Sciences, Chimie Paristech-CNRS, PSL University, F-75231 Paris Cedex 05, France;* orcid.org/0000-0002-1967-2769; Email: frederic.labat@chimieparistech.psl.eu

Authors

Luca Brugnoli − *Dipartimento di Scienze Chimiche e Geologiche, Università di Modena e Reggio Emilia, I-41125 Modena, Italy; Institute of Chemistry for Health and Life Sciences, Chimie Paristech-CNRS, PSL University, F-75231 Paris Cedex 05, France*

Maria Cristina Menziani − *Dipartimento di Scienze Chimiche e Geologiche, Università di Modena e Reggio Emilia, I-41125 Modena, Italy;* orcid.org/0000-0003-3428-5297

Carlo Adamo − *Institute of Chemistry for Health and Life Sciences, Chimie Paristech-CNRS, PSL University, F-75231 Paris Cedex 05, France; Institut Universitaire de France, F-75005 Paris, France;* orcid.org/0000-0002-2638-2735

Complete contact information is available at: https://pubs.acs.org/10.1021/acs.jpcc.0c09080

Author Contributions

L.B. performed all the simulations and wrote the manuscript. A.P. contributed to the definition of the theoretical framework and of the models to be used, read, and revised the manuscript. M.C.M. read and revised the manuscript. C.A. contributed to the definition of the theoretical framework and of the models to be used, read, and revised the manuscript. F.L. revised the work and the manuscript.

Notes

The authors declare no competing financial interest.

■ ACKNOWLEDGMENTS

The authors acknowledge the use of computational resources at Très Grand Centre de Calcul (TGCC) provided by GENCI through project A0030810135 and at Consorzio Interuniversitario del Nord-Est per il Calcolo Automatico (CINECA) provided by ISCRA through project IsC68. A.P. thanks the University of Modena and Reggio-Emilia for supporting this work by granting the internal project (Fondo di Ateneo per la Ricerca, FAR2016) entitled "Innovative (oxide-based) materials and methods for fuel cell electrodes implementation".

■ REFERENCES

(1) Libuda, J.; Freund, H.-J. Molecular Beam Experiments on Model Catalysts. *Surf. Sci. Rep.* **2005**, *57*, 157−298.

(2) *Current Trends of Surface Science and Catalysis*; Park, J. Y., Ed.; Springer New York: New York, NY, 2014.

(3) Bell, A. T. The Impact of Nanoscience on Heterogeneous Catalysis. *Science* **2003**, *299*, 1688−1691.

(4) Kim, M. J.; Han, G.-H.; Lee, S. H.; Jung, H. W.; Choung, J. W.; Kim, C. H.; Lee, K.-Y. CeO_2 Promoted Ag/TiO_2 Catalyst for Soot Oxidation with Improved Active Oxygen Generation and Delivery Abilities. *J. Hazard. Mater.* **2020**, *384*, 121341.

(5) Grabchenko, M. V.; Mamontov, G. V.; Zaikovskii, V. I.; La Parola, V.; Liotta, L. F.; Vodyankina, O. V. The Role of Metal−Support Interaction in Ag/CeO_2 Catalysts for CO and Soot Oxidation. *Appl. Catal., B* **2020**, *260*, 118148.

(6) Wang, H.; Luo, S.; Zhang, M.; Liu, W.; Wu, X.; Liu, S. Roles of Oxygen Vacancy and O− in Oxidation Reactions over CeO_2 and Ag/CeO_2 Nanorod Model Catalysts. *J. Catal.* **2018**, *368*, 365−378.

(7) Grabchenko, M.; Mikheeva, N.; Mamontov, G.; Salaev, M.; Liotta, L.; Vodyankina, O. Ag/CeO_2 Composites for Catalytic Abatement of CO, Soot and VOCs. *Catalysts* **2018**, *8*, 285.

(8) Guerra-Que, Z.; Torres-Torres, G.; Pérez-Vidal, H.; Cuauhtémoc-López, I.; Espinosa de los Monteros, A.; Beltramini, J. N.; Frías-Márquez, D. M. Silver Nanoparticles Supported on Zirconia−Ceria for the Catalytic Wet Air Oxidation of Methyl Tert-Butyl Ether. *RSC Adv.* **2017**, *7*, 3599−3610.

(9) Zhang, X.; Qu, Z.; Li, X.; Wen, M.; Quan, X.; Ma, D.; Wu, J. Studies of Silver Species for Low-Temperature CO Oxidation on Ag/SiO_2 Catalysts. *Sep. Purif. Technol.* **2010**, *72*, 395−400.

(10) Aneggi, E.; Llorca, J.; de Leitenburg, C.; Dolcetti, G.; Trovarelli, A. Soot Combustion over Silver-Supported Catalysts. *Appl. Catal., B* **2009**, *91*, 489−498.

(11) Murrell, L. L.; Carlin, R. T. Silver on Ceria: An Example of a Highly Active Surface Phase Oxide Carbon Oxidation Catalyst. *J. Catal.* **1996**, *159*, 479−490.
(12) Buendía, F.; Anzaldo, A. T.; Vital, C.; Beltrán, M. R. O_2 Activation by AuAg Clusters on a Defective (100)MgO Surface. *J. Chem. Phys.* **2020**, *152*, 024303.
(13) Shimizu, K.-i.; Kawachi, H.; Komai, S.-i.; Yoshida, K.; Sasaki, Y.; Satsuma, A. Carbon Oxidation with Ag/Ceria Prepared by Self-Dispersion of Ag Powder into Nano-Particles. *Catal. Today* **2011**, *175*, 93−99.
(14) Pan, C.-J.; Tsai, M.-C.; Su, W.-N.; Rick, J.; Akalework, N. G.; Agegnehu, A. K.; Cheng, S.-Y.; Hwang, B.-J. Tuning/Exploiting Strong Metal-Support Interaction (SMSI) in Heterogeneous Catalysis. *J. Taiwan Inst. Chem. Eng.* **2017**, *74*, 154−186.
(15) Sun, Y.-N.; Giordano, L.; Goniakowski, J.; Lewandowski, M.; Qin, Z.-H.; Noguera, C.; Shaikhutdinov, S.; Pacchioni, G.; Freund, H.-J. The Interplay between Structure and CO Oxidation Catalysis on Metal-Supported Ultrathin Oxide Films. *Angew. Chem., Int. Ed.* **2010**, *49*, 4418−4421.
(16) Diebold, U. The Surface Science of Titanium Dioxide. *Surf. Sci. Rep.* **2003**, *48*, 53−229.
(17) Zhen-Ping, Q.; Xiao-Dong, Z.; Dan, C.; Xin-Yong, L.; Meng, W.; Yi, W.; Ding, M.; Jing-Jing, W. Effect of CeO_2 on the Silver Species and Its Catalytic Activity for CO Oxidation. *DICP OpenIR* **2011**, *32*, 1605−1609.
(18) Shimizu, K.-i.; Kawachi, H.; Satsuma, A. Study of Active Sites and Mechanism for Soot Oxidation by Silver-Loaded Ceria Catalyst. *Appl. Catal., B* **2010**, *96*, 169−175.
(19) Cacciatore, M.; Rutigliano, M.; Billing, G. D. Eley-Rideal and Langmuir-Hinshelwood Recombination Coefficients for Oxygen on Silica Surfaces. *J. Thermophys. Heat Transfer* **1999**, *13*, 195−203.
(20) Atkins, P. W.; De Paula, J. *Physical Chemistry: Thermodynamics, Structure, and Change*, 10th ed.; W.H. Freeman: New York, 2014.
(21) Paier, J.; Penschke, C.; Sauer, J. Oxygen Defects and Surface Chemistry of Ceria: Quantum Chemical Studies Compared to Experiment. *Chem. Rev.* **2013**, *113*, 3949−3985.
(22) Yin, W.-J.; Wen, B.; Zhou, C.; Selloni, A.; Liu, L.-M. Excess Electrons in Reduced Rutile and Anatase TiO_2. *Surf. Sci. Rep.* **2018**, *73*, 58−82.
(23) Aneggi, E.; Boaro, M.; de Leitenburg, C.; Dolcetti, G.; Trovarelli, A. Insights into the Redox Properties of Ceria-Based Oxides and Their Implications in Catalysis. *J. Alloys Compd.* **2006**, *408*−*412*, 1096−1102.
(24) Bagheri, S.; Muhd Julkapli, N.; Bee Abd Hamid, S. Titanium Dioxide as a Catalyst Support in Heterogeneous Catalysis. *Sci. World J.* **2014**, *2014*, 1−21.
(25) Dahl, M.; Liu, Y.; Yin, Y. Composite Titanium Dioxide Nanomaterials. *Chem. Rev.* **2014**, *114*, 9853−9889.
(26) Huang, M.; Fabris, S. Role of Surface Peroxo and Superoxo Species in the Low-Temperature Oxygen Buffering of Ceria: Density Functional Theory Calculations. *Phys. Rev. B: Condens. Matter Mater. Phys.* **2007**, *75*, 081404.
(27) Conesa, J. C. Surface Anion Vacancies on Ceria: Quantum Modelling of Mutual Interactions and Oxygen Adsorption. *Catal. Today* **2009**, *143*, 315−325.
(28) Chen, H.-T.; Chang, J.-G.; Chen, H.-L.; Ju, S.-P. Identifying the O_2 Diffusion and Reduction Mechanisms on CeO_2 Electrolyte in Solid Oxide Fuel Cells: A DFT + U Study. *J. Comput. Chem.* **2009**, *30*, 2433−2442.
(29) Teng, B.-T.; Lang, J.-J.; Wen, X.-D.; Zhang, C.; Fan, M.; Harris, H. G. O_2 Adsorption and Oxidative Activity on Gold-Based Catalysts with and without a Ceria Support. *J. Phys. Chem. C* **2013**, *117*, 18986−18993.
(30) Wang, J.; Liu, M.; Lin, M. Oxygen Reduction Reactions in the SOFC Cathode of Ag/CeO_2. *Solid State Ionics* **2006**, *177*, 939−947.
(31) Preda, G.; Migani, A.; Neyman, K. M.; Bromley, S. T.; Illas, F.; Pacchioni, G. Formation of Superoxide Anions on Ceria Nanoparticles by Interaction of Molecular Oxygen with Ce^{3+} Sites. *J. Phys. Chem. C* **2011**, *115*, 5817−5822.
(32) Preda, G.; Pacchioni, G. Formation of Oxygen Active Species in Ag-Modified CeO_2 Catalyst for Soot Oxidation: A DFT Study. *Catal. Today* **2011**, *177*, 31−38.
(33) Yang, C.; Yu, X.; Heißler, S.; Weidler, P. G.; Nefedov, A.; Wang, Y.; Wöll, C.; Kropp, T.; Paier, J.; Sauer, J. O_2 Activation on Ceria Catalysts—The Importance of Substrate Crystallographic Orientation. *Angew. Chem., Int. Ed.* **2017**, *56*, 16399−16404.
(34) Schilling, C.; Ganduglia-Pirovano, M. V.; Hess, C. Experimental and Theoretical Study on the Nature of Adsorbed Oxygen Species on Shaped Ceria Nanoparticles. *J. Phys. Chem. Lett.* **2018**, *9*, 6593−6598.
(35) Rasmussen, M. D.; Molina, L. M.; Hammer, B. Adsorption, Diffusion, and Dissociation of Molecular Oxygen at Defected TiO_2(110): A Density Functional Theory Study. *J. Chem. Phys.* **2004**, *120*, 988−997.
(36) Wang, Y.; Pillay, D.; Hwang, G. S. Dynamics of Oxygen Species on Reduced TiO_2 (110) Rutile. *Phys. Rev. B: Condens. Matter Mater. Phys.* **2004**, *70*, 193410.
(37) Chrétien, S.; Metiu, H. O_2 Evolution on a Clean Partially Reduced Rutile TiO_2(110) Surface and on the Same Surface Precovered with Au1 and Au2: The Importance of Spin Conservation. *J. Chem. Phys.* **2008**, *129*, 074705.
(38) Linh, N. H.; Nguyen, T. Q.; Diño, W. A.; Kasai, H. Effect of Oxygen Vacancy on the Adsorption of O_2 on Anatase TiO_2(001): A DFT-Based Study. *Surf. Sci.* **2015**, *633*, 38−45.
(39) Xu, H.; Tong, S. Y. Interaction of O2 with Reduced Rutile TiO_2(110) Surface. *Surf. Sci.* **2013**, *610*, 33−41.
(40) Li, Y.-F.; Selloni, A. Theoretical Study of Interfacial Electron Transfer from Reduced Anatase TiO_2(101) to Adsorbed O_2. *J. Am. Chem. Soc.* **2013**, *135*, 9195−9199.
(41) Setvín, M.; Aschauer, U.; Scheiber, P.; Li, Y.-F.; Hou, W.; Schmid, M.; Selloni, A.; Diebold, U. Reaction of O_2 with Subsurface Oxygen Vacancies on TiO_2 Anatase (101). *Science* **2013**, *341*, 988−991.
(42) Li, Y.-F.; Aschauer, U.; Chen, J.; Selloni, A. Adsorption and Reactions of O_2 on Anatase TiO_2. *Acc. Chem. Res.* **2014**, *47*, 3361−3368.
(43) Wu, X.; Selloni, A.; Lazzeri, M.; Nayak, S. K. Oxygen Vacancy Mediated Adsorption and Reactions of Molecular Oxygen on the TiO_2 (110) Surface. *Phys. Rev. B: Condens. Matter Mater. Phys.* **2003**, *68*, 241402.
(44) Jia, C.; Zhang, G.; Zhong, W.; Jiang, J. A First-Principle Study of Synergized O_2 Activation and CO Oxidation by Ag Nanoparticles on TiO_2(101) Support. *ACS Appl. Mater. Interfaces* **2016**, *8*, 10315−10323.
(45) Fabris, S.; de Gironcoli, S.; Baroni, S. Electron Localization in Pure and Defective Ceria by a Unified LDA+ U Approach. **20003**, ArXiv Prepr. Cond-Mat0312601.
(46) Morgan, B. J.; Watson, G. W. A DFT+U Description of Oxygen Vacancies at the TiO_2 Rutile (110) Surface. *Surf. Sci.* **2007**, *601*, 5034−5041.
(47) Pacchioni, G. First Principles Calculations on Oxide-Based Heterogeneous Catalysts and Photocatalysts: Problems and Advances. *Catal. Lett.* **2015**, *145*, 80−94.
(48) Paier, J. Hybrid Density Functionals Applied to Complex Solid Catalysts: Successes, Limitations, and Prospects. *Catal. Lett.* **2016**, *146*, 861−885.
(49) Paier, J.; Marsman, M.; Kresse, G. Why Does the B3LYP Hybrid Functional Fail for Metals? *J. Chem. Phys.* **2007**, *127*, 024103.
(50) Janthon, P.; Luo, S.; Kozlov, S. M.; Viñes, F.; Limtrakul, J.; Truhlar, D. G.; Illas, F. Bulk Properties of Transition Metals: A Challenge for the Design of Universal Density Functionals. *J. Chem. Theory Comput.* **2014**, *10*, 3832−3839.
(51) Dovesi, R.; Erba, A.; Orlando, R.; Zicovich-Wilson, C. M.; Civalleri, B.; Maschio, L.; Rérat, M.; Casassa, S.; Baima, J.; Salustro, S.; Kirtman, B. Quantum-Mechanical Condensed Matter Simulations with CRYSTAL. *Wiley Interdiscip. Rev.: Comput. Mol. Sci.* **2018**, *8*, No. e1360.

https://dx.doi.org/10.1021/acs.jpcc.0c09080
J. Phys. Chem. C 2020, 124, 25917−25930

(52) Adamo, C.; Barone, V. Toward Reliable Density Functional Methods without Adjustable Parameters: The PBE0 Model. *J. Chem. Phys.* **1999**, *110*, 6158−6170.
(53) Brugnoli, L.; Ferrari, A. M.; Civalleri, B.; Pedone, A.; Menziani, M. C. Assessment of Density Functional Approximations for Highly Correlated Oxides: The Case of CeO_2 and Ce_2O_3. *J. Chem. Theory Comput.* **2018**, *14*, 4914−4927.
(54) Labat, F.; Baranek, P.; Domain, C.; Minot, C.; Adamo, C. Density Functional Theory Analysis of the Structural and Electronic Properties of TiO_2 Rutile and Anatase Polytypes: Performances of Different Exchange-Correlation Functionals. *J. Chem. Phys.* **2007**, *126*, 154703.
(55) Brugnoli, L.; Pedone, A.; Menziani, M. C.; Adamo, C.; Labat, F. H_2 Dissociation and Water Evolution on Silver-Decorated CeO_2(111): A Hybrid Density Functional Theory Investigation. *J. Phys. Chem. C* **2019**, *123*, 25668−25679.
(56) Tosoni, S.; Pacchioni, G. Trends in Adhesion Energies of Gold on MgO(100), Rutile TiO_2(110), and CeO_2(111) Surfaces: A Comparative DFT Study. *J. Phys. Chem. C* **2017**, *121*, 28328−28338.
(57) Dovesi, R.; Saunders, V. R.; Roetti, C.; Orlando, R.; Zicovich-Wilson, C. M.; Pascale, F.; Civalleri, B.; Doll, K.; Harrison, N. M.; Bush, I. J.; D'Arco, P.; Llunell, M.; Causà, M.; Noël, Y.; Maschio, L.; Erba, A.; Rerat, M.; Casassa, S. *CRYSTAL 17 User's Manual*; University of Torino: Torino, 2017; 2017.
(58) Grimme, S. Semiempirical GGA-Type Density Functional Constructed with a Long-Range Dispersion Correction. *J. Comput. Chem.* **2006**, *27*, 1787−1799.
(59) Grimme, S.; Antony, J.; Ehrlich, S.; Krieg, H. A Consistent and Accurate Ab Initio Parametrization of Density Functional Dispersion Correction (DFT-D) for the 94 Elements H-Pu. *J. Chem. Phys.* **2010**, *132*, 154104.
(60) Albuquerque, A. R.; Bruix, A.; Illas, F. A DFT Study on Ce-Doped Anatase TiO2: Nature of Ce3+ and Ti3+ Centers Triggered by Oxygen Vacancy Formation. *J. Phys. Chem. C* **2014**, *118*, 9677.
(61) Dolg, M.; Stoll, H.; Savin, A.; Preuss, H. Energy-Adjusted Pseudopotentials for the Rare Earth Elements. *Theor. Chim. Acta* **1989**, *75*, 173−194.
(62) Graciani, J.; Márquez, A. M.; Plata, J. J.; Ortega, Y.; Hernández, N. C.; Meyer, A.; Zicovich-Wilson, C. M.; Sanz, J. F. Comparative Study on the Performance of Hybrid DFT Functionals in Highly Correlated Oxides: The Case of CeO_2 and Ce_2O_3. *J. Chem. Theory Comput.* **2011**, *7*, 56−65.
(63) Thakkar, A. J.; Koga, T.; Saito, M.; Hoffmeyer, R. E. Double and Quadruple Zeta Contracted Gaussian Basis Sets for Hydrogen through Neon. *Int. J. Quantum Chem.* **1993**, *48*, 343−354.
(64) Labat, F.; Baranek, P.; Adamo, C. Structural and Electronic Properties of Selected Rutile and Anatase TiO_2 Surfaces: An Ab Initio Investigation. *J. Chem. Theory Comput.* **2008**, *4*, 341−352.
(65) Erba, A.; El-Kelany, Kh. E.; Ferrero, M.; Baraille, I.; Rérat, M. Piezoelectricity of $SrTiO_3$: An Ab Initio Description. *Phys. Rev. B: Condens. Matter Mater. Phys.* **2013**, *88*, 035102.
(66) Andrae, D.; Häußermann, U.; Dolg, M.; Stoll, H.; Preuß, H. Energy-Adjusted <Emphasis Type="Italic">ab Initio</Emphasis> Pseudopotentials for the Second and Third Row Transition Elements. *Theor. Chim. Acta* **1990**, *77*, 123−141.
(67) Doll, K.; Harrison, N. M. Theoretical Study of Chlorine Adsorption on the Ag(111) Surface. *Phys. Rev. B: Condens. Matter Mater. Phys.* **2001**, *63*, 165410.
(68) van Duijneveldt, F. B.; van Duijneveldt-van de Rijdt, J. G. C. M.; van Lenthe, J. H. State of the Art in Counterpoise Theory. *Chem. Rev.* **1994**, *94*, 1873−1885.
(69) Bungay, S. D.; Poirier, R. A.; Charron, R. J. Optimization of Transition State Structures Using Genetic Algorithms. *J. Math. Chem.* **2000**, *28*, 389−401.
(70) Simons, J.; Nichols, J. Strategies for Walking on Potential Energy Surfaces Using Local Quadratic Approximations. *Int. J. Quantum Chem.* **1990**, *38*, 263−276.
(71) Luches, P.; Pagliuca, F.; Valeri, S.; Illas, F.; Preda, G.; Pacchioni, G. Nature of Ag Islands and Nanoparticles on the CeO_2 (111) Surface. *J. Phys. Chem. C* **2012**, *116*, 1122−1132.
(72) Tosoni, S.; Chen, H.-Y. T.; Ruiz Puigdollers, A.; Pacchioni, G. TiO_2 and ZrO_2 in Biomass Conversion: Why Catalyst Reduction Helps. *Philos. Trans. R. Soc., A* **2018**, *376*, 20170056.
(73) Benedetti, F.; Luches, P.; Spadaro, M. C.; Gasperi, G.; D'Addato, S.; Valeri, S.; Boscherini, F. Structure and Morphology of Silver Nanoparticles on the (111) Surface of Cerium Oxide. *J. Phys. Chem. C* **2015**, *119*, 6024−6032.
(74) Chen, D. A.; Bartelt, M. C.; Seutter, S. M.; McCarty, K. F. Small, Uniform, and Thermally Stable Silver Particles on TiO_2(110)-(1×1). *Surf. Sci.* **2000**, *464*, L708−L714.
(75) Luo, K.; St Clair, T. P.; Lai, X.; Goodman, D. W. Silver Growth on TiO_2(110) (1 × 1) and (1 × 2). *J. Phys. Chem. B* **2000**, *104*, 3050−3057.
(76) Pacchioni, G. Electronic Interactions and Charge Transfers of Metal Atoms and Clusters on Oxide Surfaces. *Phys. Chem. Chem. Phys.* **2013**, *15*, 1737.
(77) Kong, D.; Wang, G.; Pan, Y.; Hu, S.; Hou, J.; Pan, H.; Campbell, C. T.; Zhu, J. Growth, Structure, and Stability of Ag on CeO_2 (111): Synchrotron Radiation Photoemission Studies. *J. Phys. Chem. C* **2011**, *115*, 6715−6725.
(78) Tereshchuk, P.; Freire, R. L. H.; Ungureanu, C. G.; Seminovski, Y.; Kiejna, A.; Da Silva, J. L. F. The Role of Charge Transfer in the Oxidation State Change of Ce Atoms in the TM_{13}−CeO_2(111) Systems (TM = Pd, Ag, Pt, Au): A DFT + U Investigation. *Phys. Chem. Chem. Phys.* **2015**, *17*, 13520−13530.
(79) Branda, M. M.; Hernández, N. C.; Sanz, J. F.; Illas, F. Density Functional Theory Study of the Interaction of Cu, Ag, and Au Atoms with the Regular CeO_2 (111) Surface. *J. Phys. Chem. C* **2010**, *114*, 1934−1941.
(80) Piotrowski, M. J.; Tereshchuk, P.; Da Silva, J. L. F. Theoretical Investigation of Small Transition-Metal Clusters Supported on the CeO_2(111) Surface. *J. Phys. Chem. C* **2014**, *118*, 21438−21446.
(81) Wagstaffe, M.; Hussain, H.; Acres, M. J.; Jones, R.; Syres, K. L.; Thomas, A. G. Structure and Reactivity of a Model Oxide Supported Silver Nanocluster Catalyst Studied by Near Ambient Pressure X-Ray Photoelectron Spectroscopy. *J. Phys. Chem. C* **2017**, *121*, 21383−21389.
(82) Lira, E.; Hansen, J. Ø.; Merte, L. R.; Sprunger, P. T.; Li, Z.; Besenbacher, F.; Wendt, S. Growth of Ag and Au Nanoparticles on Reduced and Oxidized Rutile TiO_2(110) Surfaces. *Top. Catal.* **2013**, *56*, 1460−1476.
(83) Hansen, J. Ø.; Lira, E.; Galliker, P.; Wang, J.-G.; Sprunger, P. T.; Li, Z.; Lægsgaard, E.; Wendt, S.; Hammer, B.; Besenbacher, F. Enhanced Bonding of Silver Nanoparticles on Oxidized TiO_2(110). *J. Phys. Chem. C* **2010**, *114*, 16964−16972.
(84) Pillay, D.; Hwang, G. S. Structure of Small Aun, Agn, and Cun Clusters (N=2−4) on Rutile TiO_2(110): A Density Functional Theory Study. *J. Mol. Struct.: THEOCHEM* **2006**, *771*, 129−133.
(85) Mazheika, A. S.; Matulis, V. E.; Ivashkevich, O. A. Adsorption of Ag4 Cluster on Stoichiometric TiO_2 (110) Surface: Quantum Chemical Study. *J. Mol. Struct.: THEOCHEM* **2009**, *909*, 75−78.
(86) Mazheika, A. S.; Matulis, V. E.; Ivashkevich, O. A. Density Functional Study of Adsorption of Agn (N=2,4,8) on Partially Reduced TiO_2 (110) Surface. *J. Mol. Struct.: THEOCHEM* **2010**, *950*, 46−52.
(87) Chen, P.-T.; Tyo, E. C.; Hayashi, M.; Pellin, M. J.; Safonova, O.; Nachtegaal, M.; van Bokhoven, J. A.; Vajda, S.; Zapol, P. Size-Selective Reactivity of Subnanometer Ag4 and Ag16 Clusters on a TiO_2 Surface. *J. Phys. Chem. C* **2017**, *121*, 6614−6625.
(88) Puigdollers, A. R.; Schlexer, P.; Pacchioni, G. Gold and Silver Clusters on TiO_2 and ZrO_2 (101) Surfaces: Role of Dispersion Forces. *J. Phys. Chem. C* **2015**, *119*, 15381−15389.
(89) Schvval, A. B.; Juan, A.; Cabeza, G. F. Theoretical Study of the Role of the Interface of Ag4 Nanoclusters Deposited on TiO_2(110) and TiO_2(101). *Appl. Surf. Sci.* **2019**, *490*, 343−351.

https://dx.doi.org/10.1021/acs.jpcc.0c09080
J. Phys. Chem. C 2020, 124, 25917−25930

(90) Krüger, P.; Jupille, J.; Bourgeois, S.; Domenichini, B.; Verdini, A.; Floreano, L.; Morgante, A. Intrinsic Nature of the Excess Electron Distribution at the TiO_2 (110) Surface. *Phys. Rev. Lett.* **2012**, *108*, 126803.
(91) Ganduglia-Pirovano, M. V.; Hofmann, A.; Sauer, J. Oxygen Vacancies in Transition Metal and Rare Earth Oxides: Current State of Understanding and Remaining Challenges. *Surf. Sci. Rep.* **2007**, *62*, 219−270.
(92) Ruiz Puigdollers, A.; Schlexer, P.; Tosoni, S.; Pacchioni, G. Increasing Oxide Reducibility: The Role of Metal/Oxide Interfaces in the Formation of Oxygen Vacancies. *ACS Catal.* **2017**, *7*, 6493−6513.
(93) Ganduglia-Pirovano, M. V.; Da Silva, J. L. F.; Sauer, J. Density-Functional Calculations of the Structure of Near-Surface Oxygen Vacancies and Electron Localization on CeO_2 (111). *Phys. Rev. Lett.* **2009**, *102*, 026101.
(94) Li, H.-Y.; Wang, H.-F.; Gong, X.-Q.; Guo, Y.-L.; Guo, Y.; Lu, G.; Hu, P. Multiple Configurations of the Two Excess 4 f Electrons on Defective CeO_2 (111): Origin and Implications. *Phys. Rev. B: Condens. Matter Mater. Phys.* **2009**, *79*, 193401.
(95) Ganduglia-Pirovano, M. V. Oxygen Defects at Reducible Oxide Surfaces: The Example of Ceria and Vanadia. In *Defects at Oxide Surfaces*; Jupille, J., Thornton, G., Eds.; Springer International Publishing: Cham, 2015; Vol. *58*, pp 149−190.
(96) Jerratsch, J.-F.; Shao, X.; Nilius, N.; Freund, H.-J.; Popa, C.; Ganduglia-Pirovano, M. V.; Burow, A. M.; Sauer, J. Electron Localization in Defective Ceria Films: A Study with Scanning-Tunneling Microscopy and Density-Functional Theory. *Phys. Rev. Lett.* **2011**, *106*, 246801.
(97) Farmer, J. A.; Campbell, C. T. Ceria Maintains Smaller Metal Catalyst Particles by Strong Metal-Support Bonding. *Science* **2010**, *329*, 933−936.
(98) Farmer, J. A.; Baricuatro, J. H.; Campbell, C. T. Ag Adsorption on Reduced CeO_2 (111) Thin Films. *J. Phys. Chem. C* **2010**, *114*, 17166−17172.
(99) Chrétien, S.; Metiu, H. Electronic Structure of Partially Reduced Rutile TiO_2 (110) Surface: Where Are the Unpaired Electrons Located? *J. Phys. Chem. C* **2011**, *115*, 4696−4705.
(100) Deskins, N. A.; Rousseau, R.; Dupuis, M. Distribution of Ti3+ Surface Sites in Reduced TiO_2. *J. Phys. Chem. C* **2011**, *115*, 7562−7572.
(101) Shibuya, T.; Yasuoka, K.; Mirbt, S.; Sanyal, B. Bipolaron Formation Induced by Oxygen Vacancy at Rutile TiO_2 (110) Surfaces. *J. Phys. Chem. C* **2014**, *118*, 9429−9435.
(102) Henderson, M. A.; Epling, W. S.; Perkins, C. L.; Peden, C. H. F.; Diebold, U. Interaction of Molecular Oxygen with the Vacuum-Annealed TiO_2(110) Surface: Molecular and Dissociative Channels. *J. Phys. Chem. B* **1999**, *103*, 5328−5337.
(103) Pushkarev, V. V.; Kovalchuk, V. I.; d'Itri, J. L. Probing Defect Sites on the CeO_2 Surface with Dioxygen. *J. Phys. Chem. B* **2004**, *108*, 5341−5348.
(104) Wu, Z.; Li, M.; Howe, J.; Meyer, H. M.; Overbury, S. H. Probing Defect Sites on CeO_2 Nanocrystals with Well-Defined Surface Planes by Raman Spectroscopy and O_2 Adsorption. *Langmuir* **2010**, *26*, 16595−16606.
(105) Choi, Y. M.; Abernathy, H.; Chen, H.-T.; Lin, M. C.; Liu, M. Characterization of O_2−CeO_2 Interactions Using In Situ Raman Spectroscopy and First-Principle Calculations. *ChemPhysChem* **2006**, *7*, 1957−1963.
(106) Zhao, Y.; Teng, B.-T.; Wen, X.-D.; Zhao, Y.; Chen, Q.-P.; Zhao, L.-H.; Luo, M.-F. Superoxide and Peroxide Species on CeO_2 (111), and Their Oxidation Roles. *J. Phys. Chem. C* **2012**, *116*, 15986−15991.
(107) Tuller, H. L.; Nowick, A. S. Small Polaron Electron Transport in Reduced CeO_2 Single Crystals. *J. Phys. Chem. Solids* **1977**, *38*, 859−867.
(108) Tan, S.; Ji, Y.; Zhao, Y.; Zhao, A.; Wang, B.; Yang, J.; Hou, J. G. Molecular Oxygen Adsorption Behaviors on the Rutile TiO_2(110)-1×1 Surface: An in Situ Study with Low-Temperature Scanning Tunneling Microscopy. *J. Am. Chem. Soc.* **2011**, *133*, 2002−2009.
(109) Epling, W. S.; Peden, C. H. F.; Henderson, M. A.; Diebold, U. Evidence for Oxygen Adatoms on TiO_2(110) Resulting from O_2 Dissociation at Vacancy Sites. *Surf. Sci.* **1998**, *412*−*413*, 333−343.
(110) Du, Y.; Dohnálek, Z.; Lyubinetsky, I. Transient Mobility of Oxygen Adatoms upon O_2 Dissociation on Reduced TiO_2(110). *J. Phys. Chem. C* **2008**, *112*, 2649−2653.
(111) Matthey, D.; Wang, J. G.; Wendt, S.; Matthiesen, J.; Schaub, R.; Laegsgaard, E.; Hammer, B.; Besenbacher, F. Enhanced Bonding of Gold Nanoparticles on Oxidized TiO_2 (110). *Science* **2007**, *315*, 1692−1696.
(112) Wendt, S.; Schaub, R.; Matthiesen, J.; Vestergaard, E. K.; Wahlström, E.; Rasmussen, M. D.; Thostrup, P.; Molina, L. M.; Lægsgaard, E.; Stensgaard, I.; Hammer, B.; Besenbacher, F. Oxygen Vacancies on TiO_2(110) and Their Interaction with H_2O and O_2: A Combined High-Resolution STM and DFT Study. *Surf. Sci.* **2005**, *598*, 226−245.
(113) Widmann, D.; Behm, R. J. Dynamic Surface Composition in a Mars-van Krevelen Type Reaction: CO Oxidation on Au/TiO_2. *J. Catal.* **2018**, *357*, 263−273.
(114) Ma, J.-B.; Xu, B.; Meng, J.-H.; Wu, X.-N.; Ding, X.-L.; Li, X.-N.; He, S.-G. Reactivity of Atomic Oxygen Radical Anions Bound to Titania and Zirconia Nanoparticles in the Gas Phase: Low-Temperature Oxidation of Carbon Monoxide. *J. Am. Chem. Soc.* **2013**, *135*, 2991−2998.
(115) Panov, G.; Dubkov, K.; Starokon, E. Active Oxygen in Selective Oxidation Catalysis. *Catal. Today* **2006**, *117*, 148−155.

https://dx.doi.org/10.1021/acs.jpcc.0c09080
J. Phys. Chem. C 2020, 124, 25917−25930